

# Properties of Hagen-Poiseuille flow in channel networks

Ana Filipa Valente<sup>1†</sup>, Rodrigo Almeida<sup>1†</sup>, Rui Dilão<sup>1\*†</sup>

<sup>1\*</sup>Department of Physics, University of Lisbon, Instituto Superior Técnico, Av. Rovisco Pais, Lisbon, 1049-001, Portugal.

\*Corresponding author(s). E-mail(s): [ruidilao@tecnico.ulisboa.pt](mailto:ruidilao@tecnico.ulisboa.pt);  
Contributing authors: [anasquintern@gmail.com](mailto:anasquintern@gmail.com);  
[rodrigo.1996.almeida@gmail.com](mailto:rodrigo.1996.almeida@gmail.com);

<sup>†</sup>These authors contributed equally to this work.

## Abstract

We derive the main properties of adaptive Hagen-Poiseuille flows in elastic microchannel networks similar to biological veins found in organisms. We demonstrate that adaptive Hagen-Poiseuille flows effectively simulate key features of *Physarum polycephalum* networks, replicating physiological out-of-equilibrium phenomena such as peristalsis and shuttle streaming, which are associated with the mechanism of nutrient transport in *Physarum*. A new topological steady state has been identified for asynchronous adaptation, supporting out-of-equilibrium laminar fluxes. Adaptive Hagen-Poiseuille flows exhibit saturation effects on the fluxes in contractile veins, as observed in both animal and artificial contractile veins. These results suggest that the non-equilibrium effects observed in *Physarum* have a hydrodynamic origin.

**Keywords:** Hagen-Poiseuille flows in networks, Biological networks, Shuttle streaming, Peristalsis, *Physarum polycephalum*

**MSC Classification:** 92-08 , 92-10 , 92C42 , 76D55 , 76B45

## 1 Introduction

Channel networks are ubiquitous structures for transportation and communication systems in nature [1]. Examples include the irrigation veins of organs and tumours [2, 3], nutrient transport channels in plant leaves [4], and adaptive channel networks in

microorganisms such as *Physarum polycephalum* [5, 6]. Additionally, they are present in transportation systems [7, 8] and electrical networks [9]. These systems can be described using graphs and compared to formal systems, such as the travelling salesman problem [10] and optimal Steiner tree geometries [11]. Such complex network optimisation problems in graph theory have important applications in physics, biology, and engineering.

*Physarum polycephalum*, commonly known as slime mould, is a protist that exhibits complex behaviour. Its body consists of several nuclei (syncytium) and an adaptive network of veins that transport endoplasmic fluid from food sources to various regions of the body. The geometry and adaptability of this network are crucial for *Physarum*'s growth and motility [12]. The vein walls of the network channels display periodic transversal oscillations, which are regulated by food sources and other external stimuli [13]. Although slime mould lacks any neural system or centralised control, it demonstrates high-level behaviour, such as selecting the shortest path between food sources in a maze [14].

To recreate and understand the dynamics of growth and movement of *Physarum*, several models have been developed to study the formation and optimisation of network paths [15–18]. These models are based on the phenomenology of Hagen-Poiseuille flows on graphs.

Some physical phenomena are inadequately explained concerning the characteristics of the formation and adaptation of channel networks in *Physarum*. This includes validating Murray's law at the branching points of channels [19, 20], the oscillations of channel radius and inversions of stream velocities (peristalsis and shuttle streaming), conductivity saturation in elastic vein networks, the non-uniqueness of steady-state solutions of adaptive Hagen-Poiseuille (H-P) flows, and both suboptimal and optimal channel lengths in steady-state solutions of H-P network flows. In these flows, adaptability is linked to the transverse elasticity of channels.

This paper focuses on the properties of the adaptive H-P flows described above, identifying the origins of these phenomena. We will follow the Hagen-Poiseuille formalism, [21], a Navier-Stokes type approach with a low Reynolds number, imposing fluid mass conservation and energy minimisation as developed by Almeida *et al* [16, 17]. In the next section, we describe the precise results of the temporal evolution of adaptive H-P flows in channel networks embedded in  $n$ -dimensional Euclidean spaces. In section 3, we derive the properties of the steady states of the channel flows and their spatial geometries, and we validate the Murray law for adaptive H-P flows at steady state. We compare the steady-state H-P flow patterns with *Physarum* patterns, analyse shuttle streaming and peristalsis, both observed in out-of-equilibrium flows. Finally, in section 4, we summarise the results of the paper.

## 2 Adaptive Hagen-Poiseuille flows on graphs: exact results

The fluid flow in elastic straight channel networks of various systems, such as in *Physarum polycephalum* or blood vessels in organisms, can be described as the flow of

viscous and incompressible fluids within a channel network, featuring multiple sources and sinks and adaptive conductivities.

A network of veins is represented by an undirected graph  $\mathcal{G} = (\mathcal{V}, E)$ , embedded in a  $n$ -dimensional Euclidean space, where  $\mathcal{V}$  is the set of  $N$  nodes or vertices with coordinates  $(x_i^1, \dots, x_i^n)$  for  $i = 1, \dots, N$ , and  $E$  is the set of  $M$  straight edges  $(i, j)$  connecting nodes  $i$  and  $j$ . We assume that the graph  $\mathcal{G}$  is connected, comprising only one component.

The graph  $\mathcal{G}$  is generated through the Delaunay triangulation of a square lattice of size  $m \times m$ , embedded in a unit square, where the coordinates of the interior points are modified using a Gaussian stochastic algorithm. The edges of  $\mathcal{G}$  represent elastic cylindrical channels that can expand or contract transversely to the flow. This network has  $K$  sources and  $R$  sinks at fixed nodes. The input or output fluid flux at node  $j$  is represented by  $S_j$ . If the network has a source at node  $j$ , then  $S_j > 0$ . If the network has a sink at node  $j$ ,  $S_j < 0$ . Otherwise,  $S_j = 0$ . As the fluid is incompressible,

$$\sum_{j=1}^N S_j = \sum_{j:\text{sources}} S_j + \sum_{j:\text{sinks}} S_j = 0, \quad (1)$$

and the volume of fluid in the network is constant.

The edge connecting node  $i$  to node  $j$  has a fixed length  $L_{ij}$  and a (variable) radius  $r_{ij}$ . Edges possess (variable) conductivities given by  $D_{ij} = \pi r_{ij}^4 / 8\eta$ , where  $\eta$  is the dynamic viscosity of the fluid, and  $\sqrt{D_{ij}} \simeq r_{ij}^2$  is proportional to the area of the channel  $(i, j)$ . The volume of the channel connecting node  $i$  to node  $j$  is expressed as  $V_{ij} = \pi r_{ij}^2 L_{ij} = \sqrt{8\pi\eta} L_{ij} \sqrt{D_{ij}}$ . Since the fluid is incompressible, the volume of fluid in the network remains constant and is given by

$$V = \sum_{(i,j) \in E} V_{ij} = \beta \sum_{(i,j) \in E} L_{ij} \sqrt{D_{ij}}, \quad (2)$$

where  $\beta = \sqrt{8\pi\eta}$ .

The Kirchhoff law determines the fluxes at every node  $j$ . As fluid flux is conserved, we have

$$\sum_{j:(i,j) \in E} Q_{ij} = S_i, \quad i = 1, \dots, N. \quad (3)$$

The H-P flux law states that the fluid flux in a cylindrical channel connecting node  $i$  to node  $j$  depends on the pressures at the nodes and is determined by the following relation:

$$Q_{ij} = D_{ij} \frac{(p_i - p_j)}{L_{ij}}. \quad (4)$$

Biological elastic channels exhibit transverse oscillations regulated by their flux [13, 22]. To describe these fluxes, we consider the network of channels  $\mathcal{G}$  filled with an incompressible fluid, where the channel conductivities possess a positive value. Assuming that all the fluxes  $S_i$  are known, the pressures  $p_i$  at the vertices are obtained by solving the Kirchhoff laws (3) via the H-P relationship (4). Furthermore, assuming that the veins are elastic and the conductivity can vary over time, we have:

**Theorem 1** ([17]) *Consider an H-P flow within a channel network described by a connected graph  $\mathcal{G}$ . Assume that the channels are elastic and that the transverse dimensions can change over time, whilst the volume  $V$  of fluid in the network remains constant. Then, the conductivities of the elastic channels change over time according to the adaptation law*

$$\frac{d}{dt} \sqrt{D_{ij}} = \alpha \frac{g(Q_{ij})}{\sum_{(k,m) \in E} L_{km} g(Q_{km})} - \sqrt{D_{ij}}, \quad (i, j) \in E, \quad (5)$$

where  $g(\cdot)$  is an arbitrary function that describes the elasticity of channels,  $\alpha = V/\beta$  is a constant, and  $t$  is a dimensionless time.

Let  $\mathcal{P} = \sum_{(i,j) \in E} Q_{ij}^2 L_{ij} / D_{ij}$  be the dissipated power of the H-P flow. To minimise the dissipated power while keeping the total volume of fluid constant, we consider the Lagrangian  $\mathcal{L} = \mathcal{P} - \lambda \left( V - \beta \sum_{(k,m) \in E} L_{km} \sqrt{D_{km}} \right)$  where  $\lambda$  is a Lagrange multiplier. Then we have:

**Theorem 2** ([17]) *Under the conditions of theorem 1, assuming that the dissipated energy per unit time of the H-P flow is at a minimum, then*

$$g(Q_{ij}) = Q_{ij}^{2/3}. \quad (6)$$

From these two theorems, the adaptive H-P flow has steady states that obey the conditions

$$D_{ij}^* = \alpha^2 \frac{Q_{ij}^{4/3}}{\left( \sum_{(k,m) \in E} L_{km} Q_{ij}^{2/3} \right)^2} \quad \text{or} \quad D_{ij}^{**} = 0. \quad (7)$$

The two theorem 1 and 2 and the steady-state condition (7) lead to the generalised Murray's law:

**Corollary 3** ([17]) *In the conditions of theorems 1 and 2, and assuming that the dissipated energy per unit time of the H-P flow is minimum, then, at steady state,*

$$\sum_{j:(i,j) \in E, Q_{ij} > 0} r_{ij}^3 = \sum_{j:(i,j) \in E, Q_{ij} < 0} r_{ij}^3, \quad (8)$$

for every node  $j$  of the graph  $\mathcal{G}$ .

With this construction, we can simulate out-of-equilibrium and steady laminar fluxes in networks of channels with fixed sources and sinks. The transverse adaptability of the network veins will establish a steady-state graph that links the sources and sinks.

### 3 Results

To study the properties of the adaptive H-P flow described by the above theorems, we restrict our simulations to channel networks represented by planar graphs embedded

in two-dimensional Euclidean space. This approach readily extends to  $n$ -dimensional Euclidean space through graph embedding.

As biological networks evolve over time and adapt to the intensity of flows, we start with graphs that have short edges resulting from a Delaunay triangulation. This triangulation is created from a distribution of nodes within a square lattice, where their positions are randomly perturbed using Gaussian noise with a standard deviation of  $\sigma = 0.5$ . The lengths of each edge  $L_{ij}$  are calculated based on the coordinates of nodes  $i$  and  $j$ . Some nodes may act as sources or sinks, and equation (1) is consistently verified. The flow is initialised with random conductivities  $D_{ij}(t = 0)$  uniformly distributed within the interval  $[1/2, 3/2]$ .

As equation (2) shows, the initial distribution of conductivities determines the total fluid volume within the network of channels, thereby influencing the value of the parameter  $\alpha = V/\beta$  in equation (5). To maintain a constant fluid volume under varying initial conditions, we first select the initial fluid volume  $V$ . For any initial selection of conductivities,  $V_0 = \beta \sum_{(i,j) \in E} L_{ij} \sqrt{D_{ij}(t = 0)}$ , we renormalise the initial conductivities to the new values

$$D'_{ij}(t = 0) = \left(\frac{V}{V_0}\right)^2 D_{ij}(t = 0). \quad (9)$$

Consequently, simulations with different initial conductivities and volumes can be compared. This renormalisation condition is essential, as steady-state flows depend on the distribution of initial conductivities.

To describe the temporal evolution of the adapted radii and fluid flows in all the network channels, we begin by calculating the initial pressures at each graph node. Next, channel conductivities are adapted according to equations (5), in time increments based on the following rules: After each time step  $\Delta t$ , new conductivities, pressures, and fluxes are computed. To determine the pressure at each node  $(i, j)$ , we define  $N$ -dimensional vectors  $\mathbf{p}$  and  $\mathbf{S}$ , whose  $i$ th entries are  $p_i$  and  $S_i$ , respectively. The system of equations (3) is rearranged into the matrix form  $\mathbf{W}\mathbf{p} = \mathbf{S}$ , where  $\mathbf{W}$  is an  $N \times N$  symmetric matrix with entries  $w_{ij} = \left(\sum_{(i,j) \in E} C_{ik}\right) \delta_{ij} - C_{ij}$ , and  $C_{ij} = D_{ij}/L_{ij}$ . We obtain the pressures at each graph node after solving this linear equation. According to equation (4), the newly adapted fluxes  $Q_{ij}$  are then derived. To facilitate these calculations, without loss of generality, we assume that the outflow node pressures are equal to zero.

We utilised the explicit Euler method to numerically integrate equations (5), with  $\Delta t = 0.1$ . Some parameters are maintained constant across all simulations, namely  $\beta = 1$ ,  $V = 100$  and  $\sum_{j \in \{\text{sources}\}} S_j = 1$ .

These steps are repeated over time until a steady state of the channel conductivities is attained. The steady state is realised when the condition

$$\max_{(i,j) \in E} |D_{ij}(n\Delta t) - D_{ij}((n-1)\Delta t)| < D_{\text{thr}} \quad (10)$$

is fulfilled. In all simulations, we chose  $D_{\text{thr}} = 5 \times 10^{-6}$ , where  $n$  is the first integer for which the inequality (10) is verified. This choice serves as the quantitative criterion

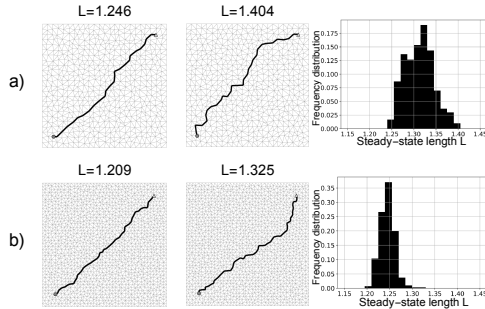


**Fig. 1** Steady states of minimum and maximum lengths of the adaptive H-P flows for one source and one sink in two graph lattices of sizes (a)  $25 \times 25$  and (b)  $40 \times 40$ . The length distribution of the steady-state graphs is also presented for each case. In a), the mean of the length distribution is  $\bar{L} = 1.312$ , and the standard deviation is  $\sigma = 0.032$ . In b),  $\bar{L} = 1.245$ , and  $\sigma = 0.017$ . The Euclidean distance between the source and sink is  $L_{\text{lin}} = 4\sqrt{2}/5 \approx 1.131$ .

for defining the stopping time of the simulations, along with the observation that the network's topology is in a topological steady state.

### 3.1 Length distributions of the steady states of the H-P flows

In all simulations, the initial distribution of nodes is inscribed within a square with a side length of side 1. The initial graph network  $\mathcal{G}$  is shown in grey, while the thickness of the black lines indicating conducting channels is proportional to the radius of the edges  $\sim D_{ij}^{1/4}$ . Source and sink nodes are represented by circles and triangles, respectively. Different choices of initial conductivities  $\{D_{ij}(t=0), (i, j) \in E\}$  may lead to different steady-state channel topologies that connect sources and sinks.

To quantify the various steady states of the adaptive H-P flows, the lengths of the steady state graphs are given by  $L = \sum_{(i,j) \in E'} L_{ij}$ , where  $E' = \{(i, j) \in E : D_{ij} > D_{\text{thr}}\}$  represents the set of conducting edges. For any  $t \geq 0$  and finite  $t$ , the graph  $\mathcal{G}$  has only one connected component, with conductivities divided into two sets of low and high values.

Figures 1 and 2 illustrate the various steady states achieved with one source and one sink inscribed within a square of side 1. In all simulations, we observed distinct steady states produced by 300 different random initial conductivity conditions. The statistics regarding the distribution of lengths of the steady-state graphs are also presented.

In figure 1, these simulations show that steady-state graphs are suboptimal in relation to the Euclidean distance between the source and the sink. By decreasing the mean lengths of the sides of Delaunay triangles (figure 1), the distribution of lengths approaches the minimum distance between the source and the sink. In the case of figure 2, this trend is also evident; however, convergence occurs over a longer timescale.

In Figure 3, we present two distinct steady states of the adaptive H-P flows for identical initial conductivities. The source and sink nodes are the same in both scenarios, but the intensities of the sources and sinks vary. In this instance, one steady state forms a connected graph tree, while the other results in a disconnected graph tree.

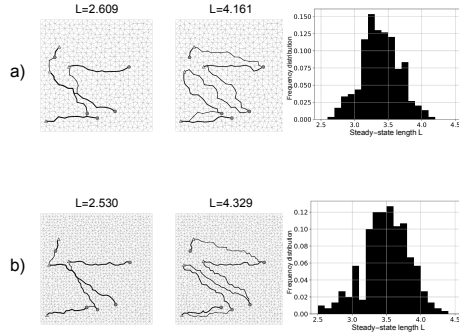


**Fig. 2** Steady states of minimum and maximum lengths of the adaptive H-P flows for five sources and four sinks in two graph lattices of sizes (a)  $25 \times 25$ , and (b)  $40 \times 40$  are presented. The steady-state graphs' length distribution is also shown in each case. In a), the mean of the length distribution is  $\bar{L} = 3.39$ , and the standard deviation is  $\sigma = 0.28$ . In b),  $\bar{L} = 3.49$ , and  $\sigma = 0.33$ .

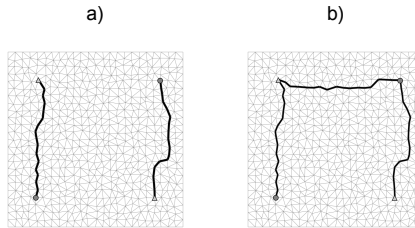


**Fig. 3** Two possible steady-state solutions of the adaptive H-P flows for two sources and two sinks in a  $25 \times 25$  graph lattice. The trees were generated using the same initial conditions. In (a),  $S_{\text{sources}} = -S_{\text{sinks}} = 0.5$ . In (b),  $S_{\text{left source}} = -S_{\text{right sink}} = 0.3$ , and  $S_{\text{right source}} = -S_{\text{left sink}} = 0.7$ .

One remarkable feature of the H-P flow is that all simulations reached a steady-state graph topology, even when we introduced stochasticity in the intensity of sources and sinks [16, 18]. In all cases, the steady-state flows obey the conditions (7). All the simulations discussed here exhibit the same qualitative features when varying all the parameters.

### 3.2 Validation of Murray's law

The generalised Murray's law (8) is a direct consequence of the set of equations used to determine the steady state of the adaptive H-P flow. However, whether it is verified during out-of-equilibrium states remains uncertain.

To verify the transient behaviour of the H-P flow, the source and sink setup shown in figure 2 was employed, with initial conductivities  $D_{ij}(t = 0) = 1$  for every pair  $(i, j) \in E$ . We selected two branching points of the steady state and analysed the

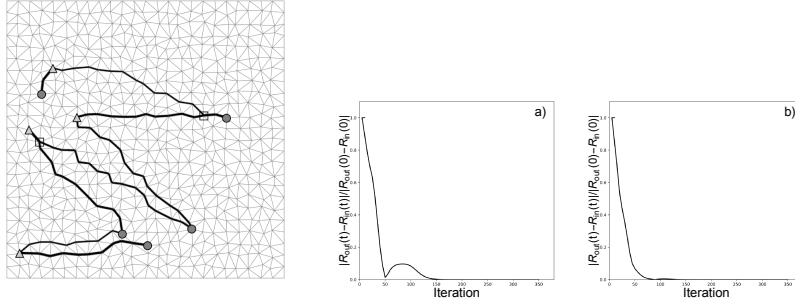


**Fig. 4** Convergence to Murray’s law at two distinct branching nodes of the steady-state subgraph. Square boxes indicate the branching nodes at a steady state of the H-P flow for the source and sink setup shown in figure 2. In a) and b), the variation of  $|R_{\text{out}}(t) - R_{\text{in}}(t)| / |R_{\text{out}}(0) - R_{\text{in}}(0)|$  over time is presented for the leftmost and rightmost branching nodes.

temporal evolution of the quantity

$$|R_{\text{out}}(t) - R_{\text{in}}(t)| := \left| \sum_{\substack{j:(i,j) \in E \\ Q_{ij} < 0}} r_{ij}^3(t) - \sum_{\substack{j:(i,j) \in E \\ Q_{ij} > 0}} r_{ij}^3(t) \right|.$$

Murray’s law is confirmed when the quantity  $|R_{\text{out}}(t) - R_{\text{in}}(t)|$  is equal to zero.

In figure 4, we illustrate the localisation of two-channel branching nodes of a steady-state H-P flow and the time evolution of  $|R_{\text{out}} - R_{\text{in}}|$  at these two branching nodes. This indicates that the generalised Murray’s law (8) is only validated for steady-state flows. Experiments with *Physarum* suggested the validity of Murray’s law [27].

### 3.3 Properties of simple networks

The formalism of adaptive H-P flows applies to straightforward networks with fixed sources and sinks, enabling fluid to flow through all the channels.

#### 3.3.1 One channel networks

We apply the conductivity adaptation algorithm to a single channel of length  $L_{12}$ , with one source and sink. Assuming that the source is located at node number 1 and the sink at node number 2, the adaptation equation

$$\frac{d}{dt} \sqrt{D_{12}} = \alpha \frac{1}{L_{12}} - \sqrt{D_{12}}, \quad (11)$$

where  $\alpha = V/\beta$ ,  $\beta = \sqrt{8\pi\eta}$ ,  $V = \beta L_{12} \sqrt{D_{12}(0)}$  and  $\eta$  is the dynamic viscosity of the fluid. The fluxes at nodes 1 and 2 are  $Q_{12} = I_1 > 0$  and  $Q_{21} = -I_1$ .

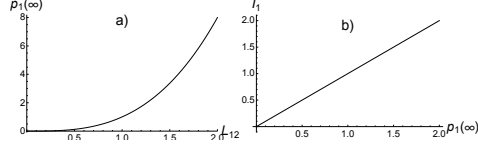


**Fig. 5** Relationship between the pressure and channel length and source fluxes in a one-channel H-P flow, with constant volume. The parameters are  $\alpha = 1$ , and  $I_1 = 1$  in a), and  $L_{12} = 1$  in b).

Equation (11) is linear, and the steady state is  $D_{12}^* = \lim_{t \rightarrow \infty} D_{12}(t) = \frac{\alpha^2}{L_{12}^2} = D_{12}(0)$ . Therefore, one-channel networks with volume conservation do not adapt as they do in H-P flows. Since  $D_{12} = \pi r_{12}^4 / (8\eta)$  and the flux is  $Q_{12} = D_{12}(p_1 - p_2) / L_{12}$ , at steady state we have

$$Q_{12}^* = D_{12}^* \frac{1}{L_{12}} (p_1(\infty) - p_2) = \frac{\alpha^2}{L_{12}^3} p_1(\infty) = I_1, \quad (12)$$

where  $p_1(\infty)$  is determined by the flux at the source  $Q_{12} = I_1$ , and we have selected  $p_2 = 0$ .

The steady-state solution  $Q_{12}^*$  in (12) indicates that, for a fixed volume  $V$ , the flux at the source increases linearly with pressure. The channel radius remains constant for every  $t \geq 0$  and is determined by  $D_{12}(0)$ .

Figure 5 shows the relationship between pressure, channel length, and source fluxes. In one-channel flows, the source flux increases with pressure.

### 3.3.2 Two channels networks

For two channels with two sinks connected to a single source (figure 6) and input flux  $I_1$ , the adaptation equations for Hagen-Poiseuille flow are

$$\begin{cases} \frac{d}{dt} \sqrt{D_{12}} = \alpha \frac{Q_{12}^{2/3}}{L_{12} Q_{12}^{2/3} + L_{13} Q_{13}^{2/3}} - \sqrt{D_{12}} \\ \frac{d}{dt} \sqrt{D_{13}} = \alpha \frac{Q_{13}^{2/3}}{L_{12} Q_{12}^{2/3} + L_{13} Q_{13}^{2/3}} - \sqrt{D_{13}} \end{cases} \quad (13)$$

with node fluxes

$$Q_{12} + Q_{13} = I_1 > 0, \quad Q_{21} = I_2 < 0, \quad Q_{31} = I_3 < 0, \quad (14)$$

and the conservation law  $I_1 + I_2 + I_3 = 0$ .

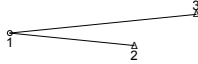


**Fig. 6** Two-channel network with one source (circle) and two sinks (triangles).

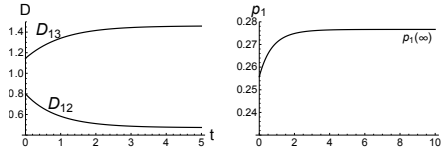


**Fig. 7** Channel conductivities and pressure at the source in two channels H-P flows, with constant volume. The parameters of the simulation are  $\alpha = 1$ ,  $I_1 = 1$ ,  $I_2 = -0.3$ ,  $I_3 = -0.7$ ,  $L_{12} = 0.4$ ,  $L_{13} = 0.6$ ,  $D_{12}(0) = 0.8$ ,  $D_{13}(0) = 1.14572$ .

By introducing the relations (14) into (13), these equations are simplified and become linear. Therefore, the steady-state conductivities are

$$D_{12}^* = \alpha^2 \frac{|I_2|^{4/3}}{(L_{12}|I_2|^{2/3} + L_{13}|I_3|^{2/3})^2} \quad (15)$$

$$D_{13}^* = \alpha^2 \frac{|I_3|^{4/3}}{(L_{12}|I_2|^{2/3} + L_{13}|I_3|^{2/3})^2},$$

where  $\alpha = V/\beta = (L_{12}\sqrt{D_{12}(0)} + L_{13}\sqrt{D_{13}(0)})$ . Therefore, since  $D_{12}^* \leq \alpha^2/L_{12}^2$  and  $D_{13}^* \leq \alpha^2/L_{13}^2$ , we have

$$\left( D_{12}^* \frac{1}{L_{12}} + D_{13}^* \frac{1}{L_{13}} \right) p_1(\infty) = I_1. \quad (16)$$

Thus, for a fixed volume  $V$  at a steady state, the pressure at the source is linearly dependent on the flux at the source. However, the flow will adjust over time, reaching the conductivity values  $D_{12}^*$  and  $D_{13}^*$ .

In figure 7, we illustrate the time evolution of the adapted conductivities and the source pressure for the two channels with fixed lengths and constant volume. Equation (16) indicates that the steady-state pressure of the source depends on the lengths of the channels.

In figure 8, we have calculated the steady-state pressures  $p_1(\infty)$  for different channel lengths and various fluxes at the source. The data indicate that an increase in pressure at the source does not correspond to an increase in flux, contrary to what has been found in the one-channel network (figure 5b)). This saturation phenomenon has been observed experimentally for contractile veins [22].

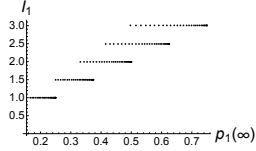


**Fig. 8** Fluxes and pressures at the source in two-channel H-P flow, akin to the experimental data in [22]. The parameters of the simulations are  $\alpha = 1$ ,  $I_1 \in [1, 3]$ ,  $I_2 = -I_1/2$ ,  $I_3 = -I_1/2$ ,  $L_{12} \in [0.5, 0.8]$ ,  $L_{12} + L_{13} = 1$ ,  $D_{12}(0) = 0.8$ ,  $D_{13}(0) = 1.14572$ .

### 3.4 Comparison between steady-state H-P flow patterns with *Physarum* patterns

The growth patterns of *Physarum polycephalum* represent a biological phenomenon employed to develop the class of models described by adaptive H-P flows on graphs.

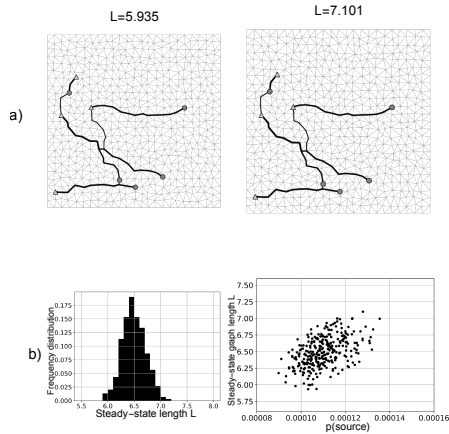
To test the development of channels in a *Physarum*-like configuration of sources and sinks, we consider one source in the centre of a square grid surrounded by 20 sinks evenly distributed along a circumference with a radius of 0.4. The fluxes are defined as  $S_{\text{source}} = 1$  and  $S_j = -1/20$  for each  $j \in \{\text{sinks}\}$ . All sources and sinks are active at all times. This configuration represents the body of a *Physarum* organism with a food source at the centre. The sinks may correspond to the peripheral regions of the plasmodium of *Physarum*, where the energy demand for growth is most critical. Over the timescale of nutrient flow, the total volume of nutrients remains conserved. This model does not account for growth by mitosis, which occurs over a longer timescale.

The shortest and longest channel graphs at steady state, obtained after adaptation, are shown in figure 9a). Figure 9b) displays the steady-state graph length distributions alongside the steady-state graph length  $L$  as a function of the pressure at the source node  $p_{\text{source}}$ . In these simulations,  $p_j = 0$  for every  $j \in \{\text{sinks}\}$ . The patterns obtained with the adaptive H-P flow resemble the pseudopodia of *Physarum* [23, figure 2b].

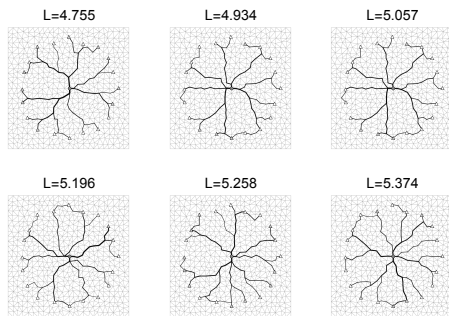
We now examine configurations resembling *Physarum*, but we consider that sinks are not active simultaneously (asynchronous adaptation). A similar adaptation mechanism to optimise railroad networks has been introduced in [26]. In particular, we consider that at each iteration, a random number of sinks  $N_{\text{sinks}}$ , between 1 and 20, is chosen to become active, while the other sinks remain inactive. In this scenario,  $S_j = -1/N_{\text{sinks}}$  for every  $j \in \{\text{active sinks}\}$ , otherwise,  $S_j = 0$  for every  $j \in \{\text{inactive sinks}\}$ . The source is always active with  $S_{\text{source}} = 1$ . This configuration also mimics the outward radial distribution of channels in *Physarum*.

Figure 10 illustrates six final states after  $3 \times 10^4$  iterations for this configuration, along with their respective lengths  $L$ , obtained using various random initial conditions. The active sinks at the end of the simulation are represented as grey triangles, while the inactive sinks are depicted as white triangles.

The states of figure 10 are not formally considered steady states because, due to asynchronous adaptation, the active sinks change with each time step, and the values of the conductivities  $D_{ij}$  never stabilise, continually fluctuating. However, the topology of the graph does attain a constant form, and the length of the graph stabilises, with



**Fig. 9** a) Steady-state configurations with minimum and maximum lengths for a *Physarum*-like arrangement of sources and sinks, for  $V = 100$ ,  $S_{\text{source}} = 1$ , and  $S_j = -1/20$ , for every  $j \in \{\text{sinks}\}$ , were obtained from 300 simulation runs with random starting conductivities. The simulations were conducted on a  $25 \times 25$  graph lattice. b) The steady-state graph length distributions and the steady-state graph length  $L$  as a function of the pressure at the source node  $p_{\text{source}}$ . The mean of the length distribution is  $\bar{L} = 6.50$  with a standard deviation of  $\sigma = 0.22$ .



**Fig. 10** The six topological steady-state channels arise from the asynchronous adaptation of *Physarum*-like configuration of sources and sinks, with  $V = 100$  and  $S_{\text{source}} = 1$ , in a  $25 \times 25$  graph lattice. The number of active sinks,  $N_{\text{extsinks}}$ , is randomly selected from the range  $1 - 20$ . Therefore,  $S_j = -1/N_{\text{active sinks}}$  for every  $j \in \{\text{active sinks}\}$ , otherwise,  $S_j = 0$  for every  $j \in \{\text{inactive sinks}\}$ . Initial conductivities are randomly chosen. The topological steady states stabilised after  $3 \times 10^4$  iterations.

$L$  decreasing over time to a minimum stable length. For this reason, the final channel configurations are referred to as topological steady states. During asynchronous adaptation, while the fluxes fluctuate over time, the topology of the channels remains constant.

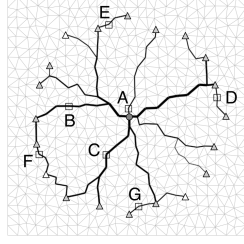


**Fig. 11** Topological steady-state configuration for the asynchronous adaptation model shown in figure 10, obtained after  $10^4$  iterations of the adaptation algorithm. To analyse the shuttle stream, we selected 7 different edges and indexed them with capital letters A-G.

One feature not explained in this approach is the development of pseudopodia transverse to the growth direction of the *Physarum*'s channels, [25, figure 2.1c] and [24].

### 3.5 Shuttle streaming

Shuttle streaming in *Physarum polycephalum* refers to the directed movement of cytoplasm within the organism, which aids in nutrient transport and other physiological processes. It occurs in various cell types across multiple organisms, including algae and slime moulds. Shuttle streaming in slime moulds features periodic cytoplasmic flow, supporting nutrient transport as the organism forms a network to optimise food access [28].

Despite extensive studies on the mechanics of cytoplasmic streaming, less is known about its biological functions and the underlying physical mechanisms. We hypothesise that shuttle streaming results from asynchronous nutrient consumption occurring locally in the *Physarum* extended cytoplasm.

To analyse shuttle streaming in *Physarum*, we began with the asynchronous adaptation algorithm from the previous section. The source in the middle is always active with  $S_{\text{source}} = 1$ , and out of the 20 possible sinks surrounding the source,  $N$  sinks are randomly selected to be active at each iteration. The source simulates a permanent food source, while the sinks represent the local consumption of resources. In this context, we conducted the simulations for  $10^4$  iterations.

After reaching the topological steady state, seven different edges were chosen. In Figure 11, we display the selected edges enclosed by square boxes. We then calculated the fluxes  $Q_{ij}$  as a function of time for these edges.

In Figure 12, we present  $Q_{ij}(t)$  for edges E and F. In edge E, we observe the inversion of the direction of flux – shuttle streaming – throughout all iterations. In edge F (as well as B, D, and G), we notice a transient shuttle streaming effect, and after a certain iteration threshold, the sign of  $Q_{ij}(t)$  stabilises. Edges A and C do not exhibit shuttle streaming during the  $10^4$  iterations.

Due to the nature of asynchronous adaptation, shuttle streaming occurs in regions of the channel network domain that are out of equilibrium, reflecting the asynchronous

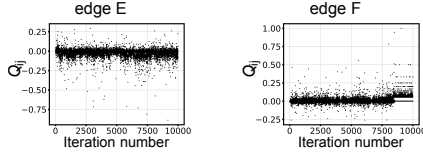


**Fig. 12** Time the evolutions of the fluxes  $Q_{ij}$  during the adaptation of H-P flow for the edges E and F, as shown in figure 11, indicate the presence of shuttle streaming during asynchronous adaptation.

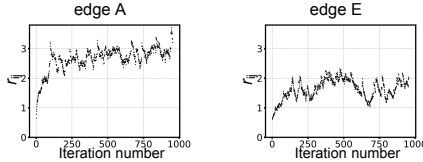


**Fig. 13** Time evolutions of the channel radius  $r_{ij}$  during the adaptation of H-P flow at edges A and E of figure 11. These simulations demonstrate the presence of peristalsis during asynchronous adaptation.

consumption of resources. In this context, shuttle streaming should be understood as an out-of-equilibrium effect.

### 3.6 Peristalsis

The adaptive H-P flow in elastic channel networks rhythmically contracts and relaxes the vein walls of the network over time. This phenomenon is known as peristalsis.

In *Physarum* growth, some elastic channels rhythmically contract and relax over time, creating an effect akin to peristalsis [29]. To evaluate the occurrence of peristalsis, we assess the channel radius  $r_{ij}(t) = (8\eta D_{ij}(t)/\pi)^{1/4}$  of the edges displayed in figure 11 over time, during the first  $10^3$  iterations of the H-P adaptation algorithm. In figure 13, we present the results for nodes A and E from figure 11. Consequently, the peristalsis phenomenon is observed during the transient process of asynchronous adaptation in the H-P flow, resulting from pressure oscillations in the channel flows associated with the Hagen-Poiseuille mechanism.

In the context of our adaptive Hagen-Poiseuille mechanism, peristalsis and shuttle streaming are only observed in simulations with asynchronous adaptation.

## 4 Conclusions

We have derived the key properties of adaptive Hagen-Poiseuille flows within channel networks, simulating the transverse elasticity of vein networks in organisms.

We have demonstrated that the tested model produces results consistent with physical observations, specifically the tendency of the adaptation to select channels near the shortest path connecting sources and sinks. The lengths of the steady-state adapted veins that connect sources and sinks are suboptimal, at least for finite triangular

geometries, which refutes the hypothesis concerning the potential for solving traveling salesman or Steiner geometry problems in graphs [30]. Additionally, Murray’s law, experimentally observed in several biological networks, is verified for steady-state H-P flow regimes.

The adaptive H-P flow description applied to simple one-channel and two-channel networks predicts the behaviour of pressure in contractile veins, as observed in various organisms. This process is associated with conductivity saturation, resulting in a threshold for fluid fluxes at the source when the pressure at the source increases while the flux remains constant.

We have compared the *Physarum*’s radial growth pattern of veins for fixed sources, along with sinks activated randomly over time – an example of asynchronous adaptation. In the latter, the pattern characteristics of *Physarum* networks were evident, showing fewer, thicker veins near food sources that branched into thinner veins as they approached the periphery (sinks).

With a permanent asynchronous adaptation of sources, a new topological steady state has been identified that supports out-of-equilibrium fluxes. In these topological steady states, the topology of the channel network and its length become fixed, but the conductivities  $D_{ij}$  do not stabilise. In these topological steady states, shuttle streaming and peristalsis are observed. Shuttle streaming appears in out-of-equilibrium regions of the channel network domain, simulating the asynchronous consumption of resources. Peristalsis arises from the transversal elasticity of channels, resulting from the pressure oscillations in the channel flows associated with the Hagen-Poiseuille mechanism. These out-of-equilibrium effects are also observed in *Physarum*. In the context of the adaptive Hagen-Poiseuille simulations shown, peristalsis and shuttle streaming are only evident in simulations with asynchronous adaptation. These results suggest that the non-equilibrium effects observed in *Physarum* have a hydrodynamic origin.

## Data availability statement

No data is associated with the manuscript.

## Author contribution statement

Author contributions to this work are as follows: R. D. developed the theoretical framework presented in this manuscript. R. A. and R. D. conducted the theoretical research. R. A. and A. F. V. performed software development and data analysis. All authors contributed to writing and reviewing the manuscript and have approved the final version for publication.

## References

- [1] T. Takahashi, *Microcirculation in Fractal Branching Networks*, Springer, Tokyo, 2014.

- [2] S. I. Rubinow, *Mathematical Problems in the Biological Sciences*, SIAM, Philadelphia, 1973.
- [3] S. Chang and M. Roper, Microvascular networks with uniform flow, *J. Theo. Bio.* **462** (2019) 48-64.
- [4] E. Katifori, G. J. Szollosi and M. O. Magnasco, Damage and fluctuations induce loops in optimal transport networks, *Phys. Rev. Lett.* **104** (2010) 048704.
- [5] W. Baumgarten, T. Ueda and M. J. B. Hauser, Plasmodial vein networks of the slime mold *Physarum polycephalum* form regular graphs, *Phys. Rev. E* **82** (2010) 046113.
- [6] C. Oettmeier, K. Brix, H.-G. Döbereiner, *Physarum polycephalum* — a new take on a classic model system, *J. of Phys. D: Appl. Phys.* **50** (2017) 413001.
- [7] A. Tero, R. Kobayashi and T. Nakagaki, *Physarum solver*: A biologically inspired method of road-network navigation. *Physica A* **363** (2006) 115-119.
- [8] D. Hu and D. Cai, Adaptation and optimization of biological transport networks, *Phys. Rev. Lett.* **111** (2013) 138701.
- [9] S. Bohn and M. O. Magnasco, Structure, scaling, and phase transition in the optimal transport network, *Phys. Rev. Lett.* **98** (2007) 088702.
- [10] L. Zhu, S.-J. Kim, M. Hara and M. Aono, Remarkable problem-solving ability of unicellular amoeboid organism and its mechanism, *R. Soc. open sci.* **5** (2018) 180396.
- [11] A. Tero, T. Nakagaki, K. Toyabe, K. Yumiki, and R. Kobayashi, A method inspired by *Physarum* for solving the Steiner problem, *Int. J. of Unconventional Computing* **6** 109-123 (2010).
- [12] W. F. Dove, J. Dee, S. Hatano, F. B. Aaugli and K.-E. Wohlfarth-Bottermann *The Molecular Biology of Physarum polycephalum*, NATO ASI series. Series A, Life Sciences, v. 106, Plenum Press, 1985.
- [13] K. E. Wohlfarth-Bottermann, Oscillatory contraction activity in *Physarum*, *J. Exp. Biol.* **81**(1) (1979) 15-32.
- [14] T. Nakagaki, H. Yamada, and Á. Tóth, Maze-solving by an amoeboid organism, *Nature*, **407** (2000) 470.
- [15] A. Tero, S. Takagi, T. Saigusa, K. Ito, D. P. Bebbler, M. D. Fricker, K. Yumiki, R. Kobayashi, and T. Nakagaki, Rules for biologically inspired adaptive network design, *Science* **327** (2010) 439-442.

- [16] R. Almeida, Formation and Optimisation of Vein Networks in Physarum, Master thesis, University of Lisbon, IST, 2021, arXiv:2305.12244v1.
- [17] R. Almeida and R. Dilão, Adaptive Hagen-Poiseuille flows on graphs, *Physica D* **426** (2022) 133322.
- [18] A. F. Valente, Applications to Biological Networks of Adaptive Hagen-Poiseuille Flow on Graphs, Master thesis, University of Lisbon, IST, 2023, arXiv:2309.10577.
- [19] C. D. Murray, The Physiological Principle of Minimum Work, *PNAS* **12** (1926) 207-214.
- [20] T. F. Sherman, On connecting large vessels to small. The meaning of Murray's law. *The Journal of General Physiology* **78**(4) (1981) 431-453.
- [21] L. Landau and E. Lefchitz, *Mécanique des fluides*, MIR, Moscou, 1971, section 17.
- [22] S. I. Rubinow and J. B. Keller, Flow of a viscous fluid through an elastic tube with applications to blood flow, *J. Theor. Biol.*, **35** (1972) 299-313.
- [23] A. Adamatzky, Developing proximity graphs by Physarums polycephalum: does the plasmodium follow the Toussaint hierarchy?, *Parallel Processing Letters* **19**(1) (2009) 105-127.
- [24] A. Adamatzky, *Physarum Machines: Computers from Slime Mould*, vol. 74, World Scientific Pub. Co. Inc. (2010).
- [25] J. Jones, *From Pattern Formation to Material Computation Multi-agent Modelling of Physarum Polycephalum*, Springer, Switzerland, 2015. Original figure from A. Adamatzky, *Physarum Machines: Computers from Slime Mould*, vol. 74, World Scientific Pub. Co. Inc. (2010).
- [26] S. Watanabe, S., A. Tero, A., Takamatsu and T. Nakagaki, Traffic optimization in railroad networks using an algorithm mimicking an amoeba-like organism, Physarum plasmodium, *Biosystems* **105** (2011) 225-232.
- [27] D. Akita, I. Kunita, M. D. Fricker, S. Kuroda, K. Sato and T. Nakagaki, Experimental models for Murray's law, *J. Phys. D: Appl. Phys.* **50** (2017) 024001.
- [28] R. E. Goldstein and J.-W. van de Meent, A physical perspective on cytoplasmic streaming, *Interface Focus* **5** (2015) 20150030.
- [29] W. Sachsenmaier, J. Blessing, B. Brauser and K. Hansen, Protoplasmic Streaming in Physarum polycephalum, *Protoplasma* **77** (1973) 381-396.
- [30] V. Bonifaci, A revised model of fluid transport optimization in Physarum polycephalum, *J. Math. Biol.* **74** (2017) 567-581.